Towards Ocean Grazer's Modular Power Take-Off System Modeling

Barradas-Berglind, J. J.; Muñoz Arias, M.; Wei, Y.; Prins, W.A.; Vakis, A.I.; Jayawardhana, B.

Published in:
20th World Congress of the International Federation of Automatic Control

DOI:
10.1016/j.ifacol.2017.08.2397

Publication date:
2017

Towards Ocean Grazer's Modular Power Take-Off System Modeling: a Port-Hamiltonian Approach

J.J. Barradas-Berglind [†,*] **M. Muñoz-Arias** [*,**] **Y. Wei** [*]
W.A. Prins [*] **A.I. Vakis** [*] **B. Jayawardhana** [*]

[*] *Faculty of Science and Engineering, University of Groningen, Groningen 9747AG, the Netherlands.*
[**] *Costa Rica Institute of Technology, Electronics Engineering School, P.O. box 159-7050- Cartago, Costa Rica.*
[†] *Corresponding author e-mail: j.d.j.barradas.berglind@rug.nl.*

Abstract: This paper presents a modular modeling framework for the Ocean Grazer's Power Take-Off (PTO) system, which operates as an array of point-absorber type devices connected to a hydraulic system. The modeling is based on the port-Hamiltonian (PH) framework that enables energy-based analysis and control of the PTO system. Firstly, a modular model of a point-absorber hydraulic system, which represents the main building block of the PTO, is presented. The model consists of wave-mechanical and hydraulic subsystems that are interconnected with a transformer-type interconnection. Secondly, we show passivity of the point-absorber hydraulic element and the accumulation of potential energy, which is due to the novel pumping mechanism of the point-absorber. Finally, we illustrate these properties through simulation results.

Keywords: Wave energy, Ocean energy, Power take-off system, Point-absorbers, Passivity

1. INTRODUCTION

Wave Energy Converters (WECs) are devices aimed at extracting the latent energy in ocean waves and transforming it into electrical energy. In recent years, a large number of near- and off-shore WECs have been proposed, whose main objective is to maximize the energy capture and minimize the loads exerted on the device. Among many proposed devices, we refer interested readers to the Pelamis WEC (Henderson, 2006), the Wavestar WEC (Hansen and Kramer, 2011), the Wave Dragon WEC (Tedd et al., 2007), the OPT WEC(Taylor, 1999) and the Ocean Grazer WEC (Vakis and Anagnostopoulos, 2016); see (Ringwood et al., 2014) for a review on WECs from a control perspective.

In particular, the novel semi-submersible Ocean Grazer (OG) energy harvesting platform has been recently proposed, which is projected to obtain its bulk energy intake from ocean waves by means of a Power Take-Off (PTO) system consisting of a collection of adaptable *point-absorber* type systems. This specific PTO, termed as the multi-piston power take-off (MP^2PTO) system, consists of an array of piston pumps with engageable pistons of different size that through a suitable control algorithm allow to extract energy from irregular waves. The main two advantages —which are not features of all WECs— of the OG-WEC are: (i) its adaptability to extract energy from ocean waves with varying heights and periods, and (ii) its loss-less storage capabilities; the former allowing for a better wave resource utilization, and the latter providing opportunities to compensate for fluctuations in power grids. The OG platform is depicted in Fig. 1a), together with a schematic of the OG-WEC in Fig. 1b). In the latter, the working principle of the OG-WEC is shown as an array of point-absorber type floater devices connected to hydraulic pumping systems, whose function is to pump working fluid from a lower to an upper reservoir.

Previous work on the OG-WEC includes (Vakis and Anagnostopoulos, 2016), where a buoy-piston-pump model was developed taking into account the hydrodynamics of the buoy and the elastohydrodynamic lubrication at the piston-cylinder interface. A simplified version of this piston-pump model was validated through a scaled down experimental test in (van Rooij et al., 2015). In (Barradas-Berglind et al., 2016), preliminary results on the energy capture of an array of point-absorbers were shown, together with a model predictive control strategy to maximize the energy extraction of the OG-WEC. In (Dijkstra et al., 2016), a revenue maximization strategy was designed, leaning on a lumped net flow dynamical model.

In this paper, we lean on a passivity-based framework in order to model the point-absorber type system that is the main building block of the OG-WEC. One framework that guarantees passivity is the port-Hamiltonian (PH) framework (Maschke and van der Schaft, 1992; Ortega et al., 2001; Duindam et al., 2009), which has been used in a wide variety of application domains, notably for its passivity preservation and non-linear controller synthesis properties; examples are electrical circuits (Jeltsema et al., 2003), hydraulic actuators (Grabmair et al., 2003), levitation systems (Fujimoto et al., 2003), robotics (Secchi et al., 2007; Munoz-Arias et al., 2014), systems with switching (Valentin et al., 2007), and power grids with market integration (Stegink et al., 2015).

Consequently, in this paper, we lean on the PH framework to investigate the energy conservation of the OG point absorber-hydraulic system, which is also beneficial since the coupling and decoupling modes of the piston-pump can be included, providing the opportunity to synthesize controllers in a more straightforward fashion. Moreover, we show the passivity property of the point-absorber hydraulic element and the accumulation of potential energy stored in the upper reservoir of the WEC. Furthermore, the modularity that the PH framework offers can be useful to interconnect several point-absorber devices in order to model the complete MP^{2}PTO system.

The remainder of the paper is organized as follows. In Section 2, we describe the wave-mechanical and hydraulic subsystems that comprise the point-absorber system. Subsequently, the port-Hamiltonian framework is described in Section 3, which is used to model the point-absorber under consideration. Accordingly, the interconnected point-absorber system in the PH framework is presented in Section 4, and numerical simulations illustrating the energy properties of the system are provided in Section 5. Lastly, conclusions are presented in Section 6.

2. OCEAN GRAZER POINT-ABSORBER MODELING

As mentioned before, a sketch of the OG-WEC is portrayed in Fig. 1b), depicting an array of point-absorbers composed of floaters B_1, B_2, B_3, B_4, a *floater blanket*, connected to pumping systems P_1, P_2, P_3, P_4. Note the check valves at the inlet of each pump, which allow flow from the lower to the upper reservoir, but prevent the reverse flow. Lastly, a turbine system T converts the stored potential energy into electrical energy. In the bottom of Fig. 1a), the MP^{2}PTO concept is illustrated together with its relation to the floater blanket, and the point-absorber (PA) element as the main building block of the OG-PTO. In this work, we focus on the modular modeling of the point-absorber element, which can be connected to other point-absorbers. Thus, in this section we describe the following subsystems: (i) a moving water body (wave) model; (ii) a mechanical subsystem consisting of a buoy-piston ensemble; (iii) a hydraulic subsystem that pumps internal fluid from a lower to an upper reservoir; and (iv) a switching coupling stage that allows energy transfer from the mechanical to the hydraulic system and prevents backflow from the upper to the lower reservoir.

2.1 Moving water body model

In order to model the wave-structure interaction in our PA-type system, we consider a model of the wave by a simple moving water body model which is described by

$$m_1 \ddot{\eta} = F_b + F_w, \tag{1}$$

where η is the displacement of the water body, m_1 describes the equivalent mass of the moving water body, F_b corresponds to the combined buoyancy and drag/friction forces due to the interaction of the buoy-piston system with the moving water mass, and finally, F_w represents the external forces. Note that in this model, the displacement in the water body is assumed to be caused by the wave propagation as well as the radiation and other hydrodynamic forces from other PAs. When we later consider the

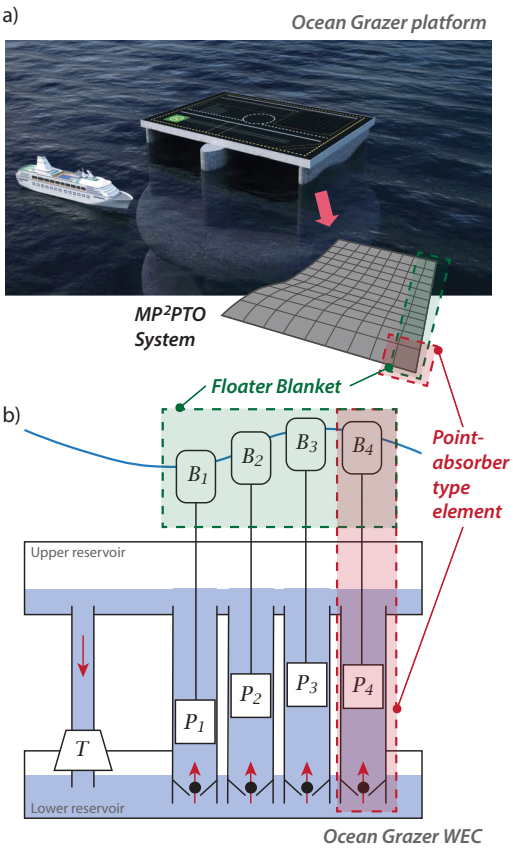

Fig. 1. a) Projected Ocean Grazer platform related to the MP^{2}PTO; b) OG-WEC schematic showing an array of floaters, a floater blanket, and the PA-type element.

interconnected PAs, we can extend the above model by including another term that couples this moving water mass with the neighboring moving water mass through spring and damper elements.

Since the moving water body in (1) is described as a mechanical system, its energy function can be generally described by

$$E_w = \frac{1}{2} c_1 \dot{\eta}^2 + \frac{1}{2} c_2 \eta^2, \tag{2}$$

where c_1 and c_2 are constants corresponding to the kinetic and potential energy. We will discuss in the following on how to relate c_1 and c_2 to the well-known wave energy characteristics from linear wave theory; see (Falnes, 2002). The energy content in a given water area A_w as derived from linear wave theory is given by

$$E_s = \frac{A_w}{16} \rho_{sw} g H_{m0}^2, \tag{3}$$

where ρ_{sw} is the sea water density, g is the gravitational acceleration constant, and H_{m0} corresponds to the estimated significant wave height.

We can relate (2) to (3) for sinusoidal waves with amplitude $H/2$ by replacing H_{m0} by $\sqrt{2}H$. Furthermore, letting $\eta(0) = H/2$ and $\dot{\eta}(0) = 0$, we obtain the potential energy constant $c_2 = k = A_w \rho_{sw} g$ that is equal to the buoyancy coefficient k, and the kinetic energy constant $c_1 = m_1$ equal to the mass of moving water.

2.2 Buoy-piston ensemble

The dynamics of the buoy-piston ensemble are given by

$$m_2\ddot{q} = -F_b - F_p, \tag{4}$$

where q is the displacement of the buoy-piston mass relative to the equilibrium position, m_2 is the equivalent buoy-piston mass, F_b corresponds to the combined buoyancy and drag forces as given before in the moving water body model and F_p is the pumping force coming from the pumping hydraulic subsystem. Next, we give a simple linear model for F_b, while the description of pumping force F_p will be given in the following subsection.

We assume a simple geometry of the buoy, such that its buoyancy and drag forces are simply proportional to the relative displacement and relative velocity between η and q, respectively. In other words, we assume that

$$F_b = -k(q-\eta) - d(\dot{q}-\dot{\eta}), \tag{5}$$

where k gives the buoyancy constant and d is the drag constant.

2.3 Pumping hydraulic system

With a reference to Fig. 2, the pumping subsystem is a hydraulic system that consists of a lower reservoir and an upper reservoir with cross-sectional areas A_l and A_u, respectively, connected through a pipe with length L_{16}. This connection is represented by two inertors $I_{12}, I_{56} > 0$, two resistors $R_{23}, R_{45} > 0$, and a pressure source $P_{34} = P_s$. To satisfy the compatibility law, the pressures in the system are related by

$$P_s = P_{65} + P_{54} + P_{32} + P_{21} + P_{16}, \tag{6}$$

where $P_s = P_{34}$ is a pressure source coupled to the buoy-piston ensemble, P_{65} is the pressure between the lower reservoir and inertor I_{56}, P_{54} is the pressure between resistor R_{45} and the piston, P_{32} is the pressure between the piston and resistor R_{23}, P_{21} is the pressure between inertor I_{12} and the upper reservoir, and lastly, P_{16} represents the pressure between upper and lower reservoirs. Furthermore, the flow of working fluid with density ρ_c from the lower to the upper reservoir is denoted by Q.

Describing the individual pressures at each component, the pressures in the inertors can be written as

$$P_{21} = I_{12}\dot{Q} + g\rho_c L_{12} \tag{7a}$$

$$P_{65} = I_{56}\dot{Q} + g\rho_c L_{56}, \tag{7b}$$

and the pressures in the resistors are given by

$$P_{32} = R_{23}Q + g\rho_c L_{23} \tag{8a}$$

$$P_{54} = R_{45}Q + g\rho_c L_{45}, \tag{8b}$$

with L_{12}, L_{56}, L_{23}, and L_{45}, being the water column heights of the system in Fig. 2. Inserting (7) and (8) into (6), yields

$$I\dot{Q} = -RQ - P_{16} + P_s - g\rho_c L_{16}, \tag{9}$$

with the equivalent inertance $I = I_{12} + I_{56}$, the equivalent resistance $R = R_{23} + R_{45}$, and the equivalent water column height $L_{16} = L_{12} + L_{23} + L_{45} + L_{56}$. Furthermore, the dynamics of pressure P_{16} can be written as the difference between the pressures at the upper and lower reservoirs as

$$\dot{P}_{16} = \frac{1}{C_{13}}Q - \left(-\frac{1}{C_{46}}Q\right), \tag{10}$$

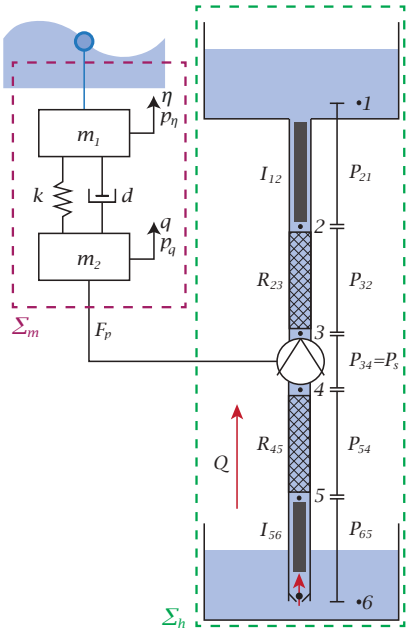

Fig. 2. Schematic of the PA-type element, depicting the mechanical and hydraulic subsystems Σ_m and Σ_h.

with the upper reservoir capacitance $1/C_{13}$ and lower reservoir capacitance $1/C_{46}$, which can be written more compactly as

$$C\dot{P}_{16} = Q, \tag{11}$$

with the equivalent capacitance $C = \frac{C_{13}C_{45}}{C_{13}+C_{45}}$.

2.4 Switched buoy-piston-pump system

The use of check valves in the piston and in the lower inlet of the lower reservoir introduces a switching behaviour in the buoy-piston-pump system, which can ideally be described in the following way. When $\dot{q} > 0$ (i.e., the buoy-piston is moving upward), the pump is activated such that both $Q > 0$ and $P_s > 0$. Otherwise, we have that both $Q = 0$ and $P_s = 0$ (i.e., the buoy-piston is moving downward). This switching mechanism in the pumping system enables us to: (i) transfer part of the kinetic energy from the water body (the upward kinetic energy) into potential energy of the working fluid, and (ii) prevent the reverse energy transfer from happening when the buoy-piston moves downward.

Therefore, depending on the velocity of the buoy-piston mass, we have the following description of the buoy-piston-pump system. For simplicity, here we assume a rigid connection between the buoy and the piston. When the working fluid is allowed to flow, we have the coupling $Q = A_c\dot{q}$ and $F_p = A_c P_s$ caused by the interaction of the buoy-piston and the pump through a given piston area. In this case, when $\dot{q} > 0$, substituting (9) into (4) together with (11) gives us the coupled buoy-piston-pump system

$$\left(m_2 + IA_c^2\right)\ddot{q} = -F_b - RA_c^2\dot{q} - A_c P_{16} - g\rho_c L_{16} A_c \tag{12a}$$

$$C\dot{P}_{16} = A_c\dot{q}, \tag{12b}$$

with F_b from (5). On the other hand, when $\dot{q} \leq 0$, we have

$$m_2\ddot{q} = -F_b \tag{13a}$$

$$C\dot{P}_{16} = 0, \tag{13b}$$

such that the buoy-piston decouples from the pump system. The above switched system equations in (12)-(13) along with the moving water body in (1) defines the basic operation of a single PA-type element in our OG-WEC. In the following section, we will discuss the port-Hamiltonian formulation of this switched system. Figure 3 shows the basic interconnection of our point-absorber system.

3. THE PORT-HAMILTONIAN FRAMEWORK

In this section, we describe the port-Hamiltonian (PH) framework introduced in (Maschke and van der Schaft, 1992). The PH framework is based on the description of a system in terms of energy variables, the usage of the port-based modeling through flow and effort variables whose product defines power, and their interconnection structure. Therefore, the PH framework allows the integration of subsystems in different domains to be combined.

The PH framework is based on the description of systems in terms of energy variables, their interconnection structure, and power ports. PH systems include a large family of physical nonlinear systems. The transfer of energy between the physical system and the environment is given through energy elements, dissipation elements, and power preserving ports; see (Maschke and van der Schaft, 1992), (van der Schaft, 2000) and (Duindam et al., 2009) for further details.

A class of PH system, introduced by (Maschke and van der Schaft, 1992), is described by

$$\Sigma = \begin{cases} \dot{x} &= \left[J\left(x\right) - R\left(x\right)\right] \dfrac{\partial H\left(x\right)}{\partial x} + g\left(x\right) u \\ y &= g\left(x\right)^{\top} \dfrac{\partial H\left(x\right)}{\partial x} \end{cases} \tag{14}$$

with states $x \in \mathbb{R}^{\mathcal{N}}$, skew-symmetric interconnection matrix $J\left(x\right) \in \mathbb{R}^{\mathcal{N}\times\mathcal{N}}$, positive semi-definite damping matrix $R\left(x\right) \in \mathbb{R}^{\mathcal{N}\times\mathcal{N}}$, and Hamiltonian $H\left(x\right) \in \mathbb{R}$. The matrix $g\left(x\right) \in \mathbb{R}^{\mathcal{N}\times\mathcal{M}}$ weights the action of the control inputs $u \in \mathbb{R}^{\mathcal{M}}$ on the system, and $(u, y) \in \mathbb{R}^{\mathcal{M}}$ with $\mathcal{M} \leq \mathcal{N}$, form a power port-pair.

For example, a class of mechanical systems with n ($\mathcal{N} = 2n$) degrees of freedom (dof) can be described as

$$\Sigma_M = \begin{cases} \begin{bmatrix} \dot{\varphi} \\ \dot{p_\varphi} \end{bmatrix} = \begin{bmatrix} 0_{n\times n} & I_{n\times n} \\ -I_{n\times n} & -D\left(\varphi, p_\varphi\right) \end{bmatrix} \begin{bmatrix} \dfrac{\partial H\left(\varphi, p_\varphi\right)}{\partial \varphi} \\ \dfrac{\partial H\left(\varphi, p_\varphi\right)}{\partial p_\varphi} \end{bmatrix} \\ \qquad\qquad + \begin{bmatrix} 0_{n\times n} \\ G\left(\varphi\right) \end{bmatrix} u \\ y \;= G\left(\varphi\right)^{\top} \dfrac{\partial H\left(\varphi, p_\varphi\right)}{\partial p_\varphi}, \end{cases} \tag{15}$$

with generalized configuration coordinates $\varphi \in \mathbb{R}^n$, generalized momenta $p_\varphi \in \mathbb{R}^n$, damping matrix $D\left(\varphi, p_\varphi\right) \in \mathbb{R}^{n\times n}$, where $D\left(\varphi, p_\varphi\right) = D\left(\varphi, p_\varphi\right)^{\top} \geq 0$, output $y \in \mathbb{R}^m$, input $u \in \mathbb{R}^m$, and input matrix $G\left(\varphi\right) \in \mathbb{R}^{n\times m}$. We assume that $G\left(\varphi\right)$ is everywhere invertible. Accordingly, the Hamiltonian of (15) is given by

$$H\left(\varphi, p_\varphi\right) = \frac{1}{2} p_\varphi^{\top} M^{-1}\left(\varphi\right) p_\varphi + V\left(\varphi\right), \tag{16}$$

where $M\left(\varphi\right) = M^{\top}\left(\varphi\right) > 0$ is the $n \times n$ inertia (generalized mass) matrix, and $V\left(\varphi\right)$ is the potential energy.

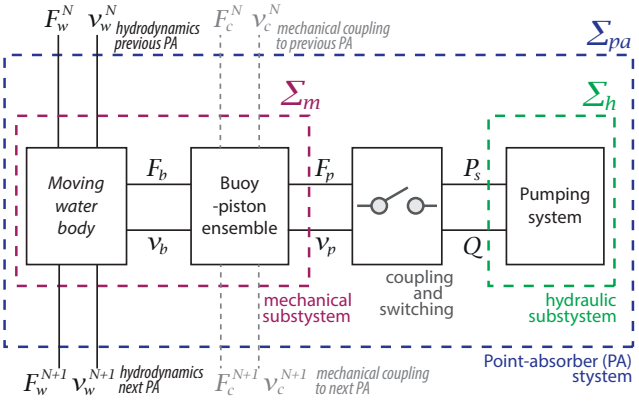

Fig. 3. Interconnected PA system Σ_{pa} schematic with its subsystems: the mechanical subsystem Σ_m, the hydraulic subsystem Σ_h, and the switching coupling stage. The potential connection to other PAs is shown through hydrodynamics and mechanical couplings.

4. PA SYSTEM IN THE PH FRAMEWORK

In this section, we describe the mechanical and hydraulic subsystems in the PH framework, i.e., Σ_m and Σ_h, respectively. Afterwards, we connect the subsystems through a transformer-type interconnection to obtain the complete description of the PA system. Two schematics of the PA system are shown in Figs. 2 and 3, where the subsystems and their interconnections can be observed.

4.1 Mechanical Subsystem

Consider the moving water body displacement η in (1) and the buoy-piston ensemble displacement q in (4) as the generalized coordinates of the mechanical subsystem. The generalized momenta of the displaced water mass and the buoy-piston ensemble mass are represented by $p_\eta = m_1\dot{\eta}$, and $p_q = m_2\dot{q}$, respectively. Subsequently, we let the state vector of the mechanical subsystem be $x_m = \left[\eta\ q\ p_\eta\ p_q\right]^{\top}$ such that the mechanical subsystem Σ_m can be written as

$$\Sigma_m = \begin{cases} \dot{x}_m = \begin{bmatrix} 0_{2\times2} & I_{2\times2} \\ -I_{2\times2} & -D_m \end{bmatrix} \dfrac{\partial H_m(x_m)}{\partial x_m} + \begin{bmatrix} 0_{2\times2} \\ I_{2\times2} \end{bmatrix} u_m \\ y_m = \begin{bmatrix} 0_{2\times2} & I_{2\times2} \end{bmatrix} \dfrac{\partial H_m(x_m)}{\partial x_m}, \end{cases} \tag{17}$$

with an external port-pair $(u_m, y_m) \in \mathbb{R}^4$ being

$$u_m = \left[u_{m,1}\ u_{m,2}\right]^{\top} = \left[F_w\ F_p\right]^{\top} \tag{18a}$$

$$y_m = \left[y_{m,1}\ y_{m,2}\right]^{\top} = \left[\frac{1}{m_1} p_\eta\ \frac{1}{m_2} p_q\right]^{\top} = \left[\dot{\eta}\ \dot{q}\right]^{\top}, \tag{18b}$$

which can be observed in Fig. 3 for $v_w = \dot{\eta}$ and $v_p = \dot{q}$. Consequently, the Hamiltonian or energy function of the mechanical subsystem Σ_m can be written as

$$H_m(x_m) = \frac{1}{2}\frac{1}{m_1} p_\eta^2 + \frac{1}{2} k(\eta - q)^2 + \frac{1}{2}\frac{1}{m_2} p_q^2 \tag{19}$$

with m_1 being the equivalent mass of the moving water body, m_2 being the mass of the buoy-piston ensemble, and $k > 0$ being the buoyancy constant. Note that $H_m(x_m) \geq 0$. Additionally, we define a dissipation term $D_m \geq 0$ as

$$D_m = \begin{bmatrix} d & -d \\ -d & d \end{bmatrix}, \tag{20}$$

with $d > 0$ being the drag coefficient between masses m_1 and m_2. Clearly, it follows from (17) that the interconnection and damping matrices, similar to the system Σ in (14), are given by

$$J_m = \begin{bmatrix} 0_{2\times2} & I_{2\times2} \\ -I_{2\times2} & 0_{2\times2} \end{bmatrix} \quad \text{and} \quad R_m = \begin{bmatrix} 0_{2\times2} & 0_{2\times2} \\ 0_{2\times2} & D_m \end{bmatrix}, \quad (21)$$

respectively. It follows that $J_m = J_m^{-\top}$, and $R_m \geq 0$ since $D_m \geq 0$. Therefore, Σ_m in (17) is in the PH framework.

4.2 Hydraulic Subsystem

Based on the power-take off system of Fig. 2, we define our generalized pressure between the upper reservoir and the lower reservoir P_{16} as described in (11), and our generalized flow rate of internal fluid Q as in (9). Accordingly, we let the state of the hydraulic system be $x_h = [P_{16}\ Q]^\top$ and we realize the Hamiltonian or energy function of the hydraulic subsystem as

$$H_h(x_h) = \frac{1}{2}CP_{16}^2 + \frac{1}{2}IQ^2 + Cg\rho_c L_{16}P_{16}, \quad (22)$$

with equivalent fluid inertance $I > 0$ and equivalent fluid capacitance $C > 0$. Note that $H_h(x_h) \geq 0$ (similarly to $H_m(x_m)$). Given the Hamiltonian function (22), together with (9) and (11), we write the hydraulic subsystem Σ_h as

$$\Sigma_h = \begin{cases} \dot{x}_h = \begin{bmatrix} 0 & {}^1/_{CI} \\ -{}^1/_{CI} & -{}^R/_{I^2} \end{bmatrix} \dfrac{\partial H_h(x_h)}{\partial x_h} + \begin{bmatrix} 0 \\ {}^1/_I \end{bmatrix} u_h \\ y_h = \begin{bmatrix} 0 & {}^1/_I \end{bmatrix} \dfrac{\partial H_h(x_h)}{\partial x_h}, \end{cases} \quad (23)$$

with an external port-pair $(u_h, y_h) \in \mathbb{R}^2$ given by

$$u_h = P_s \quad (24a)$$
$$y_h = Q. \quad (24b)$$

as it can be seen in Fig. 2. Clearly, it follows from (23) that the interconnection and damping matrices (similar to the system Σ in (14)) are given by

$$J_h = \begin{bmatrix} 0 & {}^1/_{CI} \\ -{}^1/_{CI} & 0 \end{bmatrix} \quad \text{and} \quad R_h = \begin{bmatrix} 0 & 0 \\ 0 & {}^R/_{I^2} \end{bmatrix}, \quad (25)$$

respectively. It follows that $J_h = J_h^{-\top}$ since ${}^1/_{CI} \geq 0$, and $R_h \geq 0$ since ${}^R/_{I^2} \geq 0$. Thus, we conclude that the system Σ_h in (23) is in the PH framework.

4.3 Interconnected System

As discussed in Section 2.4, there is a switching behavior in the piston and the lower inlet of the hydraulic subsystem, which allows the transfer of kinetic energy from the mechanical subsystem to the hydraulic subsystem and prevents the reverse energy transfer, effectively storing potential energy in the upper reservoir of the hydraulic subsystem. We formalize the previous through the function

$$\sigma(\dot{q}, F_p) = \sigma(y_{m,2}, u_{m,2}) = \begin{cases} 1, & \text{for } y_{m,2} \text{ and } u_{m,2} > 0 \\ 0, & \text{otherwise} \end{cases} \quad (26)$$

such that the hydraulic system becomes

$$\Sigma_h : \begin{cases} \dot{x}_h = (\sigma J_h - \sigma D_h) \dfrac{\partial H_h(x_h)}{\partial x_h} + \begin{bmatrix} 0 \\ {}^{\sigma^2}/_I \end{bmatrix} u_h \\ y_h = \begin{bmatrix} 0 & {}^{\sigma^2}/_I \end{bmatrix} \dfrac{\partial H_h(x_h)}{\partial x_h}, \end{cases} \quad (27)$$

while the mechanical subsystem Σ_m remains the same as given in (17). The interconnection between Σ_m and Σ_h is then defined by

$$u_{m,2} = -\sigma A_c u_h \quad (28a)$$
$$\sigma y_h = A_c y_{m,2}. \quad (28b)$$

Note that we do not consider the usual input-output interconnection where the output of one system is connected to the input of the other system. Instead, we interconnect the ports $(y_{m,2}, u_{m,2})$ and (y_h, u_h) as a *transformer* (van der Schaft and Jeltsema, 2014, p.19). Hence, using (26), for $\sigma = 1$ the mechanical subsystem Σ_m and the hydraulic subsystem Σ_h are coupled, whereas for $\sigma = 0$ we have

$$u_{m,2} = 0 \quad (29a)$$
$$0 = A_c y_{m,2}, \quad (29b)$$

effectively decoupling Σ_h from Σ_m (i.e., $F_p = 0$ and $\dot{q} = 0$).

For this interconnected switched system, the PA system Σ_{pa}, the external port is $(y_{m,1}, u_{m,1}) = (\dot{\eta}, F_w)$. One can check that, if we consider the Hamiltonian of the interconnected system as

$$H_{pa}(x_m, x_h) = H_m(x_m) + H_h(x_h), \quad (30)$$

then we have the passivity property of the interconnected system as shown in the following proposition.

Proposition 1. The point-absorber system Σ_{pa} resulting of the interconnection of the mechanical subsystem Σ_m and the hydraulic subsystem Σ_h through (28) is passive with respect to the external port $(y_{m,1}, u_{m,1})$.

Proof. According to (Willems, 1972), passivity is characterized by a dissipation inequality which guarantees that the product of the external ports is larger or equal to the derivative of a storage or energy function. In our case, we consider the external port $(y_{m,1}, u_{m,1}) = (\dot{\eta}, F_w)$ and the storage as the Hamiltonian of the interconnected system $H_{pa}(x_m, x_h)$ in (30) such that

$$\dot{H}_{pa}(x_m, x_h) \leq y_{m,1}u_{m,1}. \quad (31)$$

Following the interconnection in (30), the Hamiltonian rate $\dot{H}_{pa}$ can be written as

$$\begin{aligned} \dot{H}_{pa} &= \dot{H}_m(x_m) + \dot{H}_h(x_h) \\ &= \frac{\partial H_m}{\partial x_m}^\top (J_m - R_m) \frac{\partial H_m}{\partial x_m} + \frac{\partial H_m}{\partial x_m}^\top \begin{bmatrix} 0_{2\times2} \\ F_w \\ F_p \end{bmatrix} \\ &\quad + \frac{\partial H_h}{\partial x_h}^\top (\sigma J_h - \sigma R_h) \frac{\partial H_h}{\partial x_h} + \frac{\partial H_h}{\partial x_h}^\top \begin{bmatrix} 0 \\ {}^{\sigma^2}/_I P_s \end{bmatrix} \\ &= -d(\dot{\eta} - \dot{q})^2 + \dot{\eta}F_w + \dot{q}F_p - \sigma RQ^2 + \sigma^2 P_s Q, \end{aligned}$$

which, after substituting the interconnection in (28), becomes

$$\begin{aligned} \dot{H}_{pa} &= -d(\dot{\eta} - \dot{q})^2 + \dot{\eta}F_w - \dot{q}\sigma A_c P_s - \sigma RQ^2 + \sigma P_s A_c \dot{q} \\ &= -d(\dot{\eta} - \dot{q})^2 + \dot{\eta}F_w - \sigma RQ^2 \leq \dot{\eta}F_w. \end{aligned}$$

Since $d, R > 0$, we can conclude that the interconnected PA system Σ_{pa} is indeed passive with respect to the external port $(y_{m,1}, u_{m,1}) = (\dot{\eta}, F_w)$. □

Note that $\dot{H}_{pa}$ has two dissipative terms, the first one due to the drag effects in the mechanical subsystem and the second one due to the resistive effects in the hydraulic subsystem. The latter is multiplied by σ, meaning that the resistive dissipation is decoupled whenever the buoy-piston is disengaged during the downward movement.

Lastly, we illustrate the energy transfer from the mechanical to the hydraulic subsystem in the following proposition, by showing that its energy function is non-decreasing (disregarding resistive terms), which demonstrates the storage of kinetic energy from the mechanical subsystem as potential energy.

Proposition 2. The Hamiltonian or energy function $H_h(x_h)$ of the loss-less (with $R = 0$) hydraulic subsystem Σ_h is non-decreasing.

Proof. The derivative of the Hamiltonian $H_h(x_h)$ with the interconnection in (28) is given by

$$\begin{aligned}\dot{H}_h &= \frac{\partial H_h}{\partial x_h}^\top (\sigma J_h - \sigma R_h)\frac{\partial H_h}{\partial x_h} + \frac{\partial H_h}{\partial x_h}^\top \begin{bmatrix} 0 \\ \sigma^2/I P_s \end{bmatrix} \\ &= -\sigma R Q^2 + \sigma^2 P_s Q,\end{aligned}$$

which due to the switching coupling becomes

$$\dot{H}_h = \begin{cases} -RQ^2 + P_s Q & \text{for } y_{m,2} \text{ and } u_{m,2} > 0 \\ 0 & \text{otherwise.} \end{cases}$$

Hence, without the disssipative resistive term RQ^2, the only remaining term is $P_s Q = P_s A_c \dot{q} > 0$ using the switching σ in (26) and the interconnection from (29). Thus, we conclude that the Hamiltonian function of the loss-less hydraulic pumping system $H_h(x_h)$ is non-decreasing. □

5. SINGLE POINT-ABSORBER SIMULATION

In this section, we illustrate the behavior and energetic properties of the interconnected PA system Σ_{pa} obtained in Section 4.3, resulting from the interconnection of the mechanical subsystem Σ_m described in Section 4.1 and the hydraulic subsystem Σ_h introduced in Section 4.2.

The simulation was run for 100 s using Matlab/Simulink and the parameters used are summarized in Table 1. Furthermore, the fluid inertances were calculated as $I_{12} = I_{56} = \rho_c L_{16}/4A_c$ and the fluid resistances according to the Hagen-Poiseuille equation as $R_{23} = R_{45} = 2\mu\pi L_{16}/A_c^2$, where μ is the dynamic viscosity of the internal fluid. Lastly, the fluid capacitances were calculated as $1/C_{13} = \rho_c g/A_u$ and $1/C_{46} = \rho_c g/A_l$. The buoyancy coefficient was calculated through the potential energy constant in (2); the drag coefficient and the moving water equivalent mass were calculated using the boundary element method NEMOH (Babarit and Delhommeau, 2015) for a buoy with rectangular cuboid geometry (7 m ×7 m ×2 m), and their resulting curves as functions of ω are depicted in Fig. 4. The used values of d and m_1 are the ones corresponding to $\omega = 0.62$ rad/s, i.e., for a wave period of 10.13 s.

We remark that in this work we consider a fixed value of the equivalent cylinder area A_c, as shown in Table 1. However, A_c could be varied and effectively be used as a control input, as done in (Barradas-Berglind et al., 2016).

The harmonic input wave force F_w used with frequency ω is shown at the top of Fig. 5. Additionally, the resulting pumping force F_p, volumetric flow Q and pressure difference P_{16} are also depicted in Fig. 5, where it can be observed that the pumping force F_p is active during the up-stroke and zero during the down-stroke of the piston-buoy ensemble. Moreover, Q is always positive, and the pressure difference P_{16} is non-decreasing, due to the accumulation of conditioned fluid in the upper reservoir.

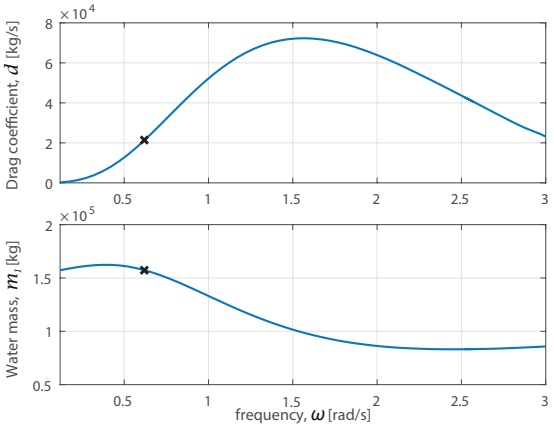

Fig. 4. Damping coefficient and equivalent water body mass. The black crosses correspond to $\omega = 0.62$rad/s.

Table 1. Model parameters.

Parameter	Value	Description [units]
g	9.81	Gravitational acceleration [m/s^2]
ρ_{sw}	1035	Sea water density at 20°C [kg/m^3]
ρ_c	998.2	Cond. fluid density at 20°C [kg/m^3]
μ	0.00089	Cond. fluid dyn. viscosity [Ns/m^2]
ω	0.62	Incoming wave frequency [rad/s]
m_1	157330.3	Displaced water eq. mass [kg]
m_2	1650	Buoy-piston ensemble eq. mass [kg]
k	497514.2	Buoyancy coefficient [kg/s^2]
d	21298	Drag coefficient [kg/s]
L_{16}	100	Pipe length [m]
A_u, A_l	49	Lower reservoir area [m^2]
A_c	0.0738	Cylinder cross section area [m^2]
I_{12}, I_{56}	338143.6	Fluid inertance [kg/m^4]
R_{23}, R_{45}	102.67	Fluid resistance [kg/m^{4}s]
$1/C_{13}$,$1/C_{46}$	0.005	Fluid capacitance [kg/m^{4}s^2]

Finally, energy transfer is illustrated in Fig 6, where the transmitted (kinetic) energy by the mechanical subsystem and the stored potential energy of the hydraulic subsystem are presented. In this figure, it can be seen that mechanical kinetic energy slowly diminishes, while being accumulated as potential energy in the upper reservoir of the hydraulic subsystem. The latter agrees with Proposition 2.

6. CONCLUSION

In this paper, we describe a buoy-piston-pump point-absorber system in the port-Hamiltonian framework, which is the main element of the Ocean Grazer WEC. Accordingly, we model both the mechanical and hydraulic subsystems separately, and we interconnect them to obtain the resulting point-absorber model. This interconnected model allows flow from the lower to the upper reservoir, but, by means of check valves, prevents backflow from the upper to the lower reservoir. We showed the passivity of the interconnected system with respect to its external port, and its energy properties were illustrated and corroborated through simulation results, which show the potential energy obtained from the incoming wave force being stored. Lastly, due to the modularity offered by the PH framework, the point-absorber type model can be used to interconnect several point-absorbers to realize the MP^{2}PTO concept of the OG-WEC. In addition, the previous may prove useful while synthesizing a control for several interconnected point-absorber devices.

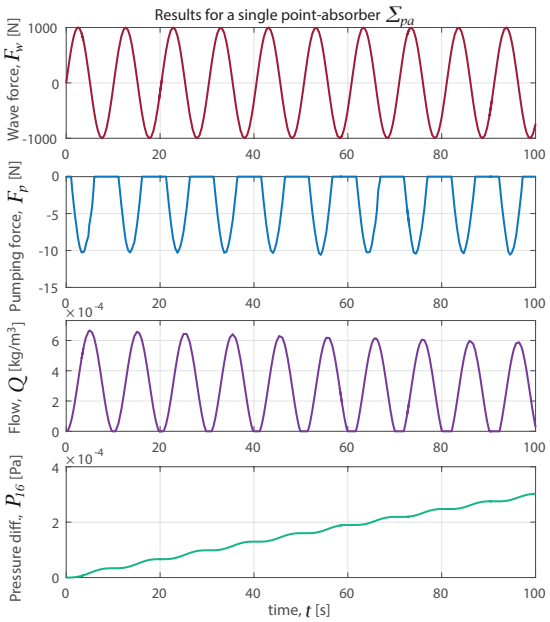

Fig. 5. Incoming wave force F_w, pumping force F_p, volumetric flow Q, and pressure difference P_{16} for Σ_{pa}.

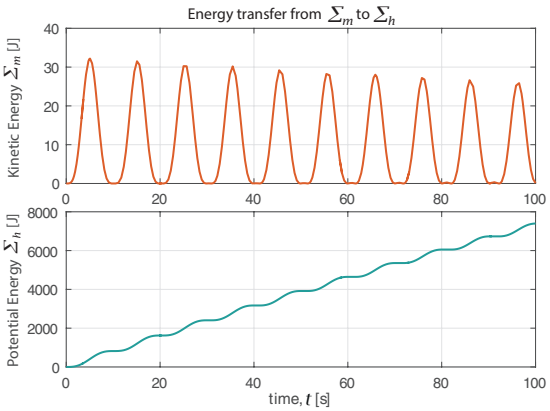

Fig. 6. Kinetic to potential energy transfer from Σ_m to Σ_h.

REFERENCES

Babarit, A. and Delhommeau, G. (2015). Theoretical and numerical aspects of the open source BEM solver NEMOH. In *Proc. of the EWTEC2015 Conference*.

Barradas-Berglind, J., Meijer, H., van Rooij, M., Clemente-Pinol, S., Galvan-Garcia, B., Prins, W., Vakis, A., and Jayawardhana, B. (2016). Energy capture optimization for an adaptive wave energy converter. In *Proc. of the RENEW2016 Conference*, 171–178.

Dijkstra, H., Barradas-Berglind, J., Meijer, H., van Rooij, M., Prins, W., Vakis, A., and Jayawardhana, B. (2016). Revenue optimization for the Ocean Grazer wave energy converter through storage utilization. In *Proc. of the RENEW2016 Conference*, 207–213.

Duindam, V., Macchelli, A., Stramigioli, S., and Bruyninckx, H. (2009). *Modeling and Control of Complex Physical Systems: The Port-Hamiltonian Approach*. Springer, Berlin, Germany.

Falnes, J. (2002). *Ocean waves and oscillating systems: linear interactions including wave-energy extraction*. Cambridge University Press.

Fujimoto, K., Sakurama, K., and Sugie, T. (2003). Trajectory tracking control of port-controlled Hamiltonian systems via generalized canonical transformations. *Automatica*, 39(12), 2059–2069.

Grabmair, G., Schlacher, K., and Kugi, A. (2003). Geometric energy based analysis and controller design of hydraulic actuators applied in rolling mills. In *2003 European Control Conference (ECC), Cambridge*.

Hansen, R.H. and Kramer, M.M. (2011). Modelling and control of the Wavestar prototype. In *Proc. of the EWTEC2011 Conference*.

Henderson, R. (2006). Design, simulation, and testing of a novel hydraulic power take-off system for the Pelamis wave energy converter. *Ren. Energy*, 31(2), 271–283.

Jeltsema, D., Ortega, R., and Scherpen, J.M. (2003). On passivity and power-balance inequalities of nonlinear RLC circuits. *IEEE Trans. on Circuits and Systems I: Fund. Theory and Applications*, 50(9), 1174–1179.

Maschke, B. and van der Schaft, A. (1992). Port-controlled Hamiltonian systems: modeling origins and system-theoretic properties. In *Proceedings of the IFAC Symposium on Nonlinear Control Systems*, 282–288.

Munoz-Arias, M., Scherpen, J.M., and Macchelli, A. (2014). An impedance grasping strategy. In *53rd IEEE Conference on Decision and Control*, 1403–1408. IEEE.

Ortega, R., van der Schaft, A.J., Mareels, I., and Maschke, B. (2001). Putting energy back in control. *IEEE Control Systems*, 21(2), 18–33.

Ringwood, J.V., Bacelli, G., and Fusco, F. (2014). Energy-maximizing control of wave-energy converters: The development of control system technology to optimize their operation. *Control Systems, IEEE*, 34(5), 30–55.

Secchi, C., Stramigioli, S., and Fantuzzi, C. (2007). *Control of interactive robotic interfaces: A port-Hamiltonian approach*, volume 29. Springer Sc. & Business Media.

Stegink, T., De Persis, C., and van der Schaft, A. (2015). A port-Hamiltonian approach to optimal frequency regulation in power grids. In *54th IEEE Conference on Decision and Control (CDC)*, 3224–3229.

Taylor, G. (1999). OPT wave power system. In *Institute of Mechanical Engineering Seminar (London)*.

Tedd, J., Kofoed, J.P., Jasinski, M., Morris, A., Friis-Madsen, E., Wisniewski, R., and Bendtsen, J.D. (2007). Advanced control techniques for WEC Wave Dragon. In *Proc. of the EWTEC2007 Conference*.

Vakis, A.I. and Anagnostopoulos, J.S. (2016). Mechanical design and modeling of a single-piston pump for the novel power take-off system of a wave energy converter. *Renewable Energy*, 96, 531–547.

Valentin, C., Magos, M., and Maschke, B. (2007). A port-Hamiltonian formulation of physical switching systems with varying constraints. *Automatica*, 43(7), 1125–1133.

van der Schaft, A. (2000). *L_2-Gain and Passivity Techniques in Nonlinear Control*. Springer, London, UK.

van der Schaft, A. and Jeltsema, D. (2014). *Port-Hamiltonian systems theory: An introductory overview*, volume 1. Now Publishers Inc.

van Rooij, M., Meijer, H., Prins, W., and Vakis, A. (2015). Experimental performance evaluation and validation of dynamical contact models of the Ocean Grazer. In *OCEANS 2015-Genova*, 1–6. IEEE.

Willems, J.C. (1972). Dissipative dynamical systems part I: General theory. *Archive for rational mechanics and analysis*, 45(5), 321–351.